On the Design of Modular Reflecting *EM* Skins for Enhanced Urban Wireless Coverage

Paolo Rocca, *Senior Member, IEEE*, Pietro Da Rù, Nicola Anselmi, *Senior Member, IEEE*, Marco Salucci, *Senior Member, IEEE*, Giacomo Oliveri, *Senior Member, IEEE*, Danilo Erricolo, *Fellow, IEEE*, and Andrea Massa, *Fellow, IEEE*

***Abstract*— The design of modular, passive, and static artificial metasurfaces to be used as electromagnetic skins (EMSs) of buildings for improving the coverage in urban millimeter-wave communication scenarios is addressed. Toward this end, an *ad hoc* design strategy is presented to determine optimal tradeoff implementation solutions that assure a suitable coverage of the areas of interest, where the signal from the base station is too weak, with the minimum complexity. More specifically, the admissible surface in the building facade is first partitioned into tiles that are the minimum-size elements of the artificial coating (i.e., the building block of an EMS). Then, the search for the optimal EMS layout (i.e., the minimum number and the positions of the tiles to be installed) is carried out with a binary multiobjective optimization method. Representative numerical results are reported and discussed to point out the features and the potentialities of the EMS solution in the smart electromagnetic environment (SEME) and the effectiveness of the proposed design method.**

***Index Terms*— Artificial materials, millimeter wave, mobile communications, multiobjective optimization, smart electromagnetic (EM) environment.**

Manuscript received 13 October 2021; revised 27 December 2021; accepted 16 January 2022. Date of publication 2 February 2022; date of current version 9 November 2022. This work was supported in part by the project CYBER-PHYSICAL ELECTROMAGNETIC VISION: Context-Aware Electromagnetic Sensing and Smart Reaction (EMvisioning) under Grant 2017HZJXSZ funded by the Italian Ministry of Education, University, and Research through the PRIN2017 Program (CUP: E64I19002530001), in part by the project SPEED under Grant 61721001 funded by the National Science Foundation of China through the Chang-Jiang Visiting Professorship Program, in part by the project Inversion Design Method of Structural Factors of Conformal Load-bearing Antenna Structure based on Desired EM Performance Interval under Grant 2017HZJXSZ funded by the National Natural Science Foundation of China, and in part by the project Research on Uncertainty Factors and Propagation Mechanism of Conformal Load-bearing Antenna Structure under Grant2021JZD-003 funded by the Department of Science and Technology of Shaanxi Province within the Program Natural Science Basic Research Plan in Shaanxi Province. *(Corresponding author: Andrea Massa.)*

Paolo Rocca is with the ELEDIA Research Center (ELEDIA@UniTN), Department of Civil, Environmental, and Mechanical Engineering (DICAM), University of Trento, 38123 Trento, Italy, and also with the ELEDIA Research Center (ELEDIA@XIDIAN) Xidian University, Xi'an, Shaanxi 710071, China (e-mail: paolo.rocca@unitn.it).

Pietro Da Rù, Nicola Anselmi, Marco Salucci, and Giacomo Oliveri are with the ELEDIA Research Center (ELEDIA@UniTN), Department of Civil, Environmental, and Mechanical Engineering (DICAM), University of Trento, 38123 Trento, Italy (e-mail: pietro.daru@unitn.it; nicola.anselmi.1@unitn.it; marco.salucci@unitn.it; giacomo.oliveri@unitn.it).

Danilo Erricolo is with the Andrew Electromagnetics Laboratory, Department of Electrical and Computer Engineering, University of Illinois Chicago, Chicago, IL 60607 USA (e-mail: derric1@uic.edu).

Andrea Massa is with the ELEDIA Research Center (ELEDIA@UniTN), Department of Civil, Environmental, and Mechanical Engineering (DICAM), University of Trento, 38123 Trento, Italy, also with the ELEDIA Research Center (ELEDIA@UESTC) School of Electronic Engineering, University of Electronic Science and Technology of China (UESTC), Chengdu 611731, China, and also with the ELEDIA Research Center (ELEDIA@TSINGHUA), Tsinghua University, Beijing 100084, China (e-mail: andrea.massa@unitn.it).

Color versions of one or more figures in this article are available at https://doi.org/10.1109/TAP.2022.3146870.

Digital Object Identifier 10.1109/TAP.2022.3146870

I. Introduction

STARTING from the first generation of cellular networks, back when the communications were analog and the portable devices heavy and cumbersome, there has always been a continuous technological push toward higher data rates, which are a mandatory requirement with the introduction of smartphones and the sharing of multimedia contents now enabled by the fast and reliable data streams of 4G and 5G communication networks [1]–[3]. Regardless of the throughput of modern communication networks, the data traffic is expected to further increase in the next years because of the massive proliferation of wireless devices and systems (e.g., smartphones, tablets, Internet-of-Things (IoT) sensors, and robots), as well as the introduction of novel applications, including, for instance, the autonomous driving [4], the tactile internet [5], and the remote control of robots [6]. All these applications will unavoidably require improved coverage (i.e., a higher level of the electromagnetic (EM) signal in the coverage area) and better quality-of-service (QoS) for mobile users/devices, as well as wireless links characterized by lower latency and higher throughput/resiliency [7], [8]. Toward this end, future mobile communication networks will have to assure more and more reliable and ubiquitous connections, everywhere and anytime, as never seen before. However, the standard solutions chosen by the operators (i.e., installing more base stations (BSs), transmitting more power, or using new frequency bands) are no longer applicable because of the too high power consumption due to the foreseen explosion of the traffic needs and the spectrum congestion [9]. Moreover, the obstacles/scatterers in the environment cannot be neglected due to the increase in the operation frequencies (e.g., millimeter waves in 5G [10]) so that the non-line-of-sight (NLOS) condition has to be taken into account since the design of the wireless network architecture.

A possible countermeasure to these issues and challenges is the "implementation" of the so-called smart EM environment (SEME) [11], where the objects and the scatterers within the

environment are considered, unlike in the past, as enablers [12] of the EM propagation and not impairments. The environment is, thus, exploited as an additional degree of freedom (DoF) for tailoring the propagation of the EM waves and to enhance the signal strength in the "blind spots," namely, the zones where the signal from the BS is too weak to support the desired throughput for users' applications [12]. By using artificial materials (e.g., engineered materials or metamaterials [13]) on the building facades or integrated within panels along the streets, the propagation of the EM waves in complex urban scenarios is controlled to fit QoS requirements and coverage targets. Passive (i.e., without active amplifiers) reconfigurable metasurfaces, which behave like intelligent reflecting surfaces (IRSs) [14]–[20], due to simple electronic devices, such as radio frequency switches [21], have been successfully installed, but they will not be massively deployed until their cost is significantly reduced.

An opposite strategy still profitably exploits the objects in the environment, without introducing additional materials, but optimizing the excitations of the array elements of the BS to generate a desired EM field distribution in the desired spots [22]. Although there are no additional costs and an installation of new hardware is not required, the opportunistic use of the BS array offers the designer a limited number of DoFs, and accurate knowledge of the surrounding scenario is also needed to assure a suitable/stable QoS.

Differently, this article is concerned with the instance of the SEME vision aimed at providing a doable large-scale solution suitable for mass production. More specifically, it proposes a method for the design of modular, passive, and static metasurfaces to build effective and low-cost EM skins (EMSs). In telecommunication engineering, the term EMS refers to a device conformal to the external surface of the object, where it is installed, which offers a set of functionalities related to the sensing and the manipulation of the EM waves [23]. A typical deployment for an EMS is over the facades of a building, which are strategic assets in an urban scenario for redirecting the impinging EM field toward areas where the signal would otherwise be weak. Starting from the selection/definition of the maximal area available on a building facade, the support of the EMS is discretized into tiles that are the elementary building blocks of an EMS. The arrangement of the tiles on the admissible surface of the facade is then optimized with a multiobjective global optimization strategy based on a binary implementation of the Non-Dominated Sorting Genetic Algorithm II (NSGA-II) [24] to yield the optimal tradeoff solutions between the best coverage of the zones of interest and the minimum number of tiles.

To the best of our knowledge, the main innovative contributions of this research work include: 1) the description, the statement, and the mathematical formalization of a novel design problem within the SEME framework; 2) the development of a customized design strategy for selecting the minimum number of tiles of the EMS that assures the coverage of the regions of interest; and 3) the synthesis of innovative tiled EMSs to be embedded in the facade of buildings for improving the EM coverage within urban millimeter-wave communication scenarios.

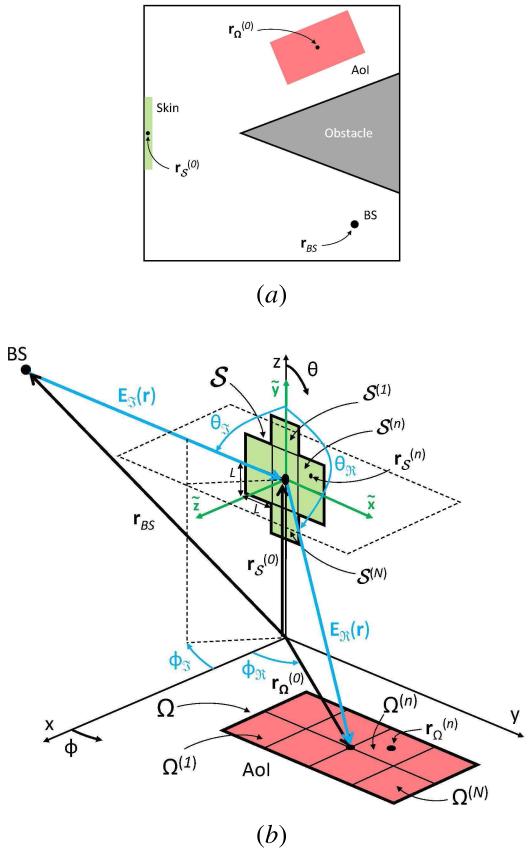

Fig. 1. *Problem geometry*. Illustrative sketches of the wireless communication scenario: (a) top view and (b) detailed zoom.

The rest of this article is organized as follows. The synthesis problem of the modular, passive, and static EMS is mathematically described and formulated in Section II, while the optimization-based design method is presented in Section III. Section IV deals with the validation and the numerical assessment of the proposed concepts and synthesis method by considering realistic urban scenarios served by a millimeter-waveband of 5G systems. Eventually, some conclusions and final remarks are drawn in Section V.

II. Mathematical Formulation

Let us consider an urban scenario [see Fig. 1(a)] where a BS serves the terminals and the devices in the surrounding environment to implement the communication network by providing wireless services to the users with a suitable QoS. Because of the presence and the configuration of the buildings, the signal from the BS is absent or too weak to guarantee a connection to the network or a sufficient throughput in some areas, $\{\Omega_b;\ b = 1, \ldots, B\}$, of the scenario at hand. In order to increase the signal strength in these "blind spots," the installation of artificial EMSs is considered.

For the sake of formulation simplicity, the case of a single "blind spot" (i.e., $B = 1$, $\Omega \leftarrow \Omega_b$), where there is neither direct nor reflected signal from the BS, is taken into account. Accordingly, only the effect of the EM field reflected from the EMS without considering the presence of the walls and

the design of a single EMS on a facade of a building are considered in this work. However, it is worthwhile pointing out that both the theoretical description and the proposed design method can be straightforwardly extended to the case with multiple skins over multiple buildings to cover multiple blind spots. With reference to such a benchmark, an area $\mathcal{S}$ on the external wall of a selected building is assumed to be located on the yz plane, subdivided into N square tiles, $\{\mathcal{S}^{(n)};\ n = 1,\ldots,N\}$ ($\bigcup_{n=1}^{N}\mathcal{S}^{(n)} = \mathcal{S}$), of equal size $\Delta\mathcal{S}$ ($\Delta\mathcal{S} = L \times L$, with L being the side length of each tile), and centered at the positions $\mathbf{r}_{\mathcal{S}}^{(n)} = y_{\mathcal{S}}^{(n)}\widehat{\mathbf{y}} + z_{\mathcal{S}}^{(n)}\widehat{\mathbf{z}}$ ($n = 1,\ldots,N$) [see Fig. 1(b)], while the BS is located at $\mathbf{r}_{BS} = x_{BS}\widehat{\mathbf{x}} + y_{BS}\widehat{\mathbf{y}} + z_{BS}\widehat{\mathbf{z}}$ in the far-field of $\mathcal{S}$.

Without loss of generality, the EM wave generated from the BS and impinging on the EMS is modeled as a monochromatic plane wave at the working frequency f with electric field [25], [26]

$$\mathbf{E}_{\Im}(\mathbf{r}) \triangleq E_{\Im}\,\widehat{\mathbf{e}}_{\Im}\,e^{-j\mathbf{k}_{\Im}\cdot\left(\mathbf{r}-\mathbf{r}_{\mathcal{S}}^{(0)}\right)} \tag{1}$$

where $E_{\Im}$ is the complex-valued wave amplitude, $\widehat{\mathbf{e}}_{\Im}$ is the complex polarization vector, and $\mathbf{k}_{\Im}$ ($\mathbf{k}_{\Im} \triangleq -k[\sin\theta_{\Im}\cos\phi_{\Im}\widehat{\mathbf{x}} + \sin\theta_{\Im}\sin\phi_{\Im}\widehat{\mathbf{y}} + \cos\theta_{\Im}\widehat{\mathbf{z}}]$) is the incident wave vector, with k being the free-space wavenumber ($k \triangleq (2\pi/\lambda)$, with λ being the wavelength at f), while $(\theta_{\Im}^{(0)}, \phi_{\Im}^{(0)})$ is the direction of arrival of the incident wave from the BS to the center of $\mathcal{S}$, $\mathbf{r}_{\mathcal{S}}^{(0)}$ ($\mathbf{r}_{\mathcal{S}}^{(0)} = y_{\mathcal{S}}^{(0)}\widehat{\mathbf{y}} + z_{\mathcal{S}}^{(0)}\widehat{\mathbf{z}}$) [see Fig. 1(b)], being $\theta_{\Im}^{(n)}\rfloor_{n=0} = \arccos((z_{BS} - z_{\mathcal{S}}^{(n)})/(|\mathbf{r}_{BS} - \mathbf{r}_{\mathcal{S}}^{(n)}|))\rfloor_{n=0}$ and $\phi_{\Im}^{(n)}\rfloor_{n=0} = \arctan((y_{BS} - y_{\mathcal{S}}^{(n)})/(x_{BS} - x_{\mathcal{S}}^{(n)}))\rfloor_{n=0} = \arctan((y_{BS} - y_{\mathcal{S}}^{(n)})/x_{BS})\rfloor_{n=0}$ since $x_{\mathcal{S}}^{(0)} = 0$.

Each tile $\mathcal{S}^{(n)}$ ($n = 1,\ldots,N$) of the EMS is illuminated from the direction $(\theta_{\Im}^{(n)}, \phi_{\Im}^{(n)})$, and it reflects the impinging wave toward a different direction $(\theta_{\Re}^{(n)}, \phi_{\Re}^{(n)})$ [$\theta_{\Re}^{(n)} = \arccos((z_{\Omega}^{(n)} - z_{\mathcal{S}}^{(0)})/(|\mathbf{r}_{\Omega}^{(n)} - \mathbf{r}_{\mathcal{S}}^{(0)}|))$, $\phi_{\Re}^{(n)} = \arctan((y_{\Omega}^{(n)} - y_{\mathcal{S}}^{(0)})/x_{\Omega}^{(n)})$] ($n = 1,\ldots,N$) by focusing the reflected beam in the point $\mathbf{r}_{\Omega}^{(n)}$ ($\mathbf{r}_{\Omega}^{(n)} = x_{\Omega}^{(n)}\widehat{\mathbf{x}} + y_{\Omega}^{(n)}\widehat{\mathbf{y}} + z_{\Omega}^{(n)}\widehat{\mathbf{z}}$, $n = 1,\ldots,N$) of the coverage region Ω, which is also called area of interest (AoI). More in detail, the AoI is assumed parallel to the xy plane (i.e., $z_{\Omega}^{(n)} = z_{\Omega}\ \forall n$), centered at $\mathbf{r}_{\Omega}^{(0)}$, and discretized into N partitions, $\{\Omega^{(n)};\ n = 1,\ldots,N\}$ (i.e., $\bigcup_{n=1}^{N}\Omega^{(n)} = \Omega$), with equal dimensions $\Delta\Omega^{(n)} = \Delta\Omega$, having barycenters at $\mathbf{r}_{\Omega}^{(n)}$ ($n = 1,\ldots,N$) along the directions of the reradiation angles [see Fig. 1(b)].

By neglecting the polarization and the reflection losses, the far-field expression of the electric field reflected from the nth ($n = 1,\ldots,N$) tile $\mathcal{S}^{(n)}$ in a generic point $\tilde{\mathbf{r}}$ of the local coordinate system[1] (see Fig. 2), $\mathbf{E}_{\Re}^{(n)}(\tilde{\mathbf{r}}) = E_{\Re}^{(n)}(\tilde{\mathbf{r}})\,\widehat{\mathbf{e}}_{\Re}$, is given by the following closed-form expression [29]:

$$\begin{aligned} E_{\Re}^{(n)}(\tilde{\mathbf{r}}) \simeq\ & -jk\eta\frac{e^{-jk\left(d_{\Im}^{(n)}+d_{\Re}^{(n)}\right)}}{4\pi\, d_{\Im}^{(n)} d_{\Re}^{(n)}}L^2 \\ & \times\left(\cos\tilde{\theta}_{\Im}^{(n)} + \cos\tilde{\theta}_{\Re}^{(n)}\right)\mathrm{sinc}\left(kL\mathcal{D}_{\tilde{x}}\right)\mathrm{sinc}\left(kL\mathcal{D}_{\tilde{y}}\right) \\ & \times e^{-j(\varphi_{\Im}+\varphi_{\Re})} \end{aligned} \tag{2}$$

[1]The following relationships between the reference and the local coordinate systems hold true: $\tilde{x} = y$, $\tilde{y} = z - z_{\mathcal{S}}^{(n)}$, and $\tilde{z} = x$.

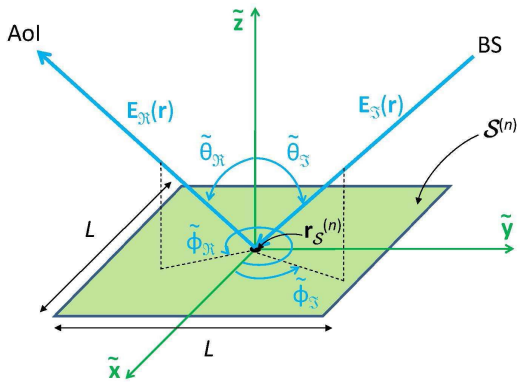

Fig. 2. *Problem geometry.* Graphical representation of the EMS local coordinate system.

where η is the free-space impedance, while $d_{\Im}^{(n)}$ and $d_{\Re}^{(n)}$ are the distances traveled by the incident wave from the BS to the barycenter of the nth ($n = 1,\ldots,N$) tile ($d_{\Im}^{(n)} = |\mathbf{r}_{BS} - \mathbf{r}_{\mathcal{S}}^{(n)}|$) and by the reflected wave from the barycenter of the nth ($n = 1,\ldots,N$) tile to the point $\mathbf{r}_{\Omega}^{(n)}$ where the peak of the reflected beam, generated from the same nth tile, is directed ($d_{\Re}^{(n)} = |\mathbf{r}_{\mathcal{S}}^{(n)} - \mathbf{r}_{\Omega}^{(n)}|$), respectively. Moreover, $\varphi_{\Im}$ is the phase associated with the modulation of the signal generated by the BS, and $\varphi_{\Re}$ is the phase term that can be engineered with the design of the surface, while $\mathcal{D}_{\tilde{x}} = \sin\tilde{\theta}\cos\tilde{\phi} - \sin\tilde{\theta}_{\Re}^{(n)}\cos\tilde{\phi}_{\Re}^{(n)}$ and $\mathcal{D}_{\tilde{y}} = \sin\tilde{\theta}\sin\tilde{\phi} - \sin\tilde{\theta}_{\Re}^{(n)}\sin\tilde{\phi}_{\Re}^{(n)}$.

To improve the coverage within the AoI by guaranteeing a suitable intensity of the signal from the BS by means of the reflection from the EMS, the following synthesis problem is formulated.

Modular Reflecting EM Skin (MREMS) Design Problem: Given an admissible skin surface $\mathcal{S}$ discretized into N square tiles $\{\mathcal{S}^{(n)};\ n = 1,\ldots,N\}$ and an AoI Ω, select the minimum number of tiles M (i.e., $M \leq N$), which reflects the EM wave from the BS toward the corresponding focusing points, $\{\mathbf{r}_{\Omega}^{(n)};\ n = 1,\ldots,M\}$, within the AoI ($\mathbf{r}_{\Omega}^{(n)} \in \Omega$), so that the power collected by a receiver at the position $\mathbf{r}_u$ of the AoI ($\mathbf{r}_u \in \Omega$), $\mathcal{P}_{\Re}(\mathbf{r}_u)$ ($\mathcal{P}_{\Re}(\mathbf{r}) \triangleq \sum_{m=1}^{M}|E_{\Re}^{(m)}(\mathbf{r})|^2$), fulfills the condition

$$\mathcal{P}_{\Re}(\mathbf{r}_u) \geq \mathcal{P}_{th} \tag{3}$$

where $\mathcal{P}_{th}$ is a user-defined coverage threshold ($\mathcal{P}_{th} \geq \mathcal{P}_{bls}$, with $\mathcal{P}_{bls}$ being the minimum level for a wireless connection).

III. MREMS Synthesis Method

The MREMS design problem is addressed through a multiobjective optimization strategy based on a binary implementation of the NSGA-II [24]. Toward this end, the presence/absence of a tile on the final EMS layout $\mathcal{S}_{opt}$ is mathematically modeled by means of a binary variable, t_n ($t_n \in \{0, 1\}$) ($n = 1,\ldots,N$). If $t_n = 1$, then the nth ($n = 1,\ldots,N$) tile $\mathcal{S}^{(n)}$ is present on the facade of the building, and it contributes to the reflection of the EM wave toward the AoI. Otherwise (i.e., $t_n = 0$), the nth ($n = 1,\ldots,N$) tile $\mathcal{S}^{(n)}$ is not

installed on the external wall of the building, which maintains its original scattering properties without contributing to the enhancement of the signal in Ω. Accordingly, an admissible layout of the EMS (i.e., an arrangement of tiles over the available surface $\mathcal{S}$) is univocally described by the binary vector $\mathbf{T}$ ($\mathbf{T} \triangleq \{t_n; n = 1, \ldots, N\}$.

In order to determine the final structure of the EMS, $\mathcal{S}_{opt}$, namely, the best subset of M tiles among the N admissible ones to be installed in $\mathcal{S}$, the problem is formulated as an optimization one by defining suitable optimization objectives aimed at quantifying the mismatch between the desired coverage (3) with that afforded by a trial EMS arrangement, $\mathbf{T}$, as well as the complexity of the final layout of the EMS, $\mathbf{T}_{opt}$. More specifically, the following two cost functions are defined. The former is the "*coverage term*," $\Phi_1(\mathbf{T})$, given by

$$\Phi_1(\mathbf{T}) \triangleq \frac{1}{U}\sum_{u=1}^{U} \frac{\left|\sum_{n=1}^{N} t_n \mathcal{P}_{\Re}^{(n)}(\mathbf{r}_u;\ \mathbf{T}) - \mathcal{P}_{th}\right|}{\mathcal{P}_{th}} \times \mathcal{H}\left\{\mathcal{P}_{th} - \sum_{n=1}^{N} t_n \mathcal{P}_{\Re}^{(n)}(\mathbf{r}_u;\ \mathbf{T})\right\} \quad (4)$$

while the latter is the "*complexity term*" defined as

$$\Phi_2(\mathbf{T}) \triangleq \frac{M}{N} \quad (5)$$

where U is the number of receivers, which are uniformly distributed inside the AoI Ω, and M ($M = \sum_{n=1}^{N} t_n$) is the number of tiles composing the EMS. Moreover, $\mathcal{H}(\cdot)$ is the Heaviside function equal to 1 when the argument is positive (i.e., $\mathcal{P}_{th} > \mathcal{P}_{\Re}(\mathbf{r}_u; \mathbf{T}) \rightarrow$ the power strength at $\mathbf{r}_u$ is below the desired value) and 0 otherwise [i.e., $\mathcal{P}_{th} \leq \mathcal{P}_{\Re}(\mathbf{r}_u; \mathbf{T}) \rightarrow$ the coverage condition (3) is fulfilled].

Since the two cost functions to be minimized impose, on the one hand, the fitting of the coverage condition (4), and, on the other hand, the reduction of the number of tiles to minimize the area/cost of the skin (5), they are by definition conflicting. Indeed, a larger number of tiles lead to a stronger electric field in Ω and vice versa. Thus, the optimization problem turns out to be natively multiobjective, and a natural solution strategy is that of defining a Pareto front of multiple optimal solutions, each being a valid tradeoff to be considered for the final implementation of the EMS on the building facade. Such a multiplicity of solutions gives to the designer the possibility of choosing the EMS layout to be implemented according to its feeling and other nonfunctional constraints (e.g., architectural and landscaping restrictions, and costs). Following such a guideline, the binary NSGA-II [24] is chosen as the optimization algorithm because of the binary nature of the design problem at hand ($\mathbf{T}$ being a binary vector) and the need of synthesizing multiple tradeoff solutions among the conflicting objectives. Moreover, due to its hill-climbing features [28], the genetic algorithm (GA) has global optimization features that are here compulsory due to the nonconvex behaviors of the cost functions. Indeed, Φ_1 and Φ_2 are noncontinuous functions also characterized by the presence of local minima (i.e., suboptimal solutions of the corresponding EMS design problem).

More in detail, the following implementation of the binary NSGA-II is taken into account.

1) *Step 0—NSGA-II Setup:* Select the number of P individuals (i.e., trial layouts of the EMS) of the GA population and set the control parameters of the NSGA-II, namely, the crossover rate, $\wp_c$, the polynomial mutation rate, $\wp_m$, the distribution index for both the crossover, $\aleph_c$, the mutation rate, $\aleph_m$, and the maximum number of iterations, I, with i being the iteration index ($i = 0, \ldots, I$).
2) *Step 1—Population Initialization ($i = 0$):* Randomly set the initial trial solutions, $\{\mathbf{T}_i^{(p)}; p = 1, \ldots, P\}$, and compute the cost function terms, $\Phi_{1,i}^{(p)} = \Phi_1(\mathbf{T}_i^{(p)})$ and $\Phi_{2,i}^{(p)} = \Phi_2(\mathbf{T}_i^{(p)})$, for each individual of the population ($p = 1, \ldots, P$).
3) *Step 2—EMS Optimization ($i = 1, \ldots, I$):* Apply the evolutionary operators of the NSGA-II to iteratively ($i \leftarrow i + 1$), generate the offsprings, $\{\mathbf{T}_i^{(p)}; p = 1, \ldots, P\}$, from the current population of parents, $\{\mathbf{T}_{i-1}^{(p)}; p = 1, \ldots, P\}$, and compute their fitness values (4) and (5). Stop the iterative process when the maximum number of iterations ($i = I$) is reached.
4) *Step 3—Final Tradeoff EMS Design:* Select the set of O trial solutions that are nondominated and belonging to the optimized Pareto front [24], $\{\mathbf{T}_{opt}^{(o)}; o = 1, \ldots, O\}$. Such solutions are ordered according to the Φ_2 cost function value, namely, $\mathbf{T}_{opt}^{(o)}\rfloor_{o=1} = \min_{o=1,\ldots,O}\{\Phi_2(\mathbf{T}_{opt}^{(o)})\}$ and $\mathbf{T}_{opt}^{(o)}\rfloor_{o=O} = \max_{o=1,\ldots,O}\{\Phi_2(\mathbf{T}_{opt}^{(o)})\}$. For a given oth ($o = 1, \ldots, O$) Pareto optimal solution, $\mathbf{T}_{opt}^{(o)}$, place the nth ($n = 1, \ldots, N$) tile $\mathcal{S}^{(n)}$ of the skin at the position $\mathbf{r}_{\mathcal{S}}^{(n)}$ on the wall of the building if $t_{n,opt}^{(o)} = 1$.

IV. Numerical Results

The objective of this section is twofold: on the one hand, the critical evaluation of the impact on the wireless coverage of using modular EMSs; on the other hand, the assessment of the effectiveness of the proposed design method by considering different scenarios and tiles while validating (2) through full-wave simulations with ANSYS HFSS [30].

As for this latter, the validation benchmark consists of a single ($N = 1$) tile located on the yz plane at the center of a Cartesian coordinate system and illuminated by a millimeter ($f = 27$ [GHz]) plane wave generated from the BS (1) that impinges with an orthogonal incidence $(\theta_{\Im}^{(1)}, \phi_{\Im}^{(1)}) = (0, 0)$ [deg] on the tile with a vertical polarized (i.e., $\widehat{\mathbf{e}}_r = \widehat{\mathbf{y}}$) electric field. The distance between the BS and the tile has been chosen equal to $d_{\Im}^{(1)} = 100$ [m] ($\rightarrow 9 \times 10^3\ \lambda$), while the side and the square area of the tile have been set to $L^{(1)} = 25\ \lambda$ and $\Delta\mathcal{S}^{(1)} \simeq 0.277 \times 0.277$ [m^2], respectively.

The realistic EMS tile of this specific example has been modeled with the ANSYS HFSS software as a metasurface defined by a lattice of unit cells uniformly space along the x- and y-axes by ($\lambda/2$). Each unit-cell is composed of a square metallic patch printed on a single-layer Rogers 3003 dielectric substrate with thickness 5.08×10^{-4} [m] [see Fig. 3(a)]. The single-tile EMS has been then designed by shaping the metallic

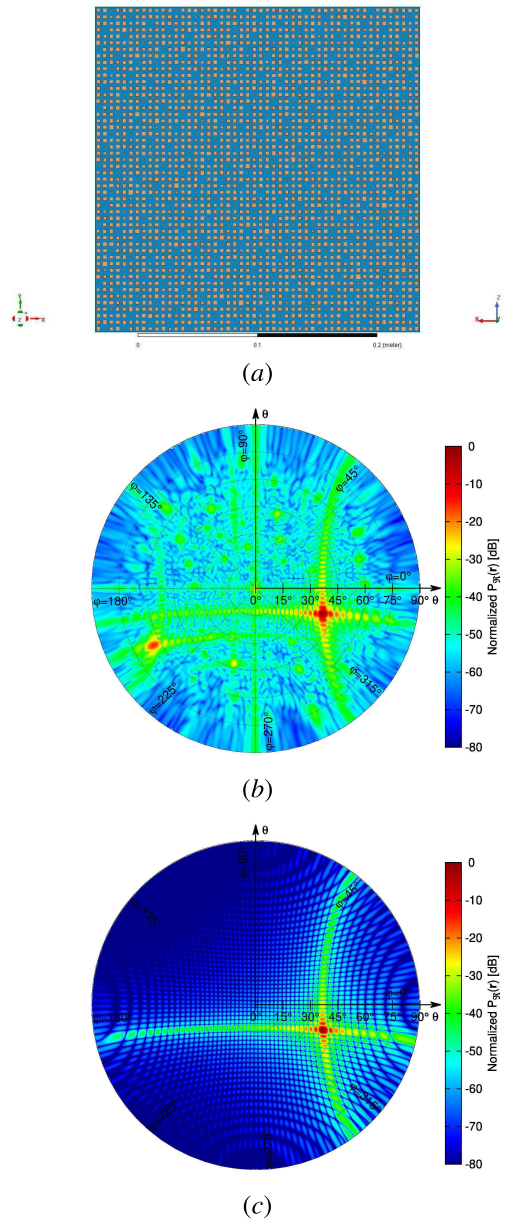

Fig. 3. *Numerical validation*. Layouts of (a) ANSYS HFSS model of the single-tile EMS and plot of (b), and (c) angular distribution of the power, $\mathcal{P}_{\Re}(\mathbf{r})$, reflected from the EMS on a sphere at a distance of 5 [m] and computed with (b) ANSYS HFSS or using (c) closed-form relationship (2).

patches of the metasurface[2] through the task-oriented multi-scale design strategy based on the system-by-design paradigm proposed in [27] so that it reflects the impinging wave toward the direction $(\theta_{\Re}^{(1)}, \phi_{\Re}^{(1)}) = (40, -20)$ [deg].

For comparison purposes, the power, $\mathcal{P}_{\Re}(\mathbf{r})$, reflected from the realistic [see Fig. 3(b)] and the ideal [see Fig. 3(c)] tiles on a sphere at a distance of 5 [m] from the skin barycenter $\mathbf{r}_{\mathcal{S}}^{(0)}$ is shown in Fig. 3. As for the reflected electric field computed in HFSS, only the copolar component is shown for the sake of comparison with the field reflected from ideal skin, which is

[2]It is worth to point out that each tile has to be different and characterized by a suitable layout of the metallic patches to enforce the required phase distribution in order to reflect the impinging wave along the desired direction.

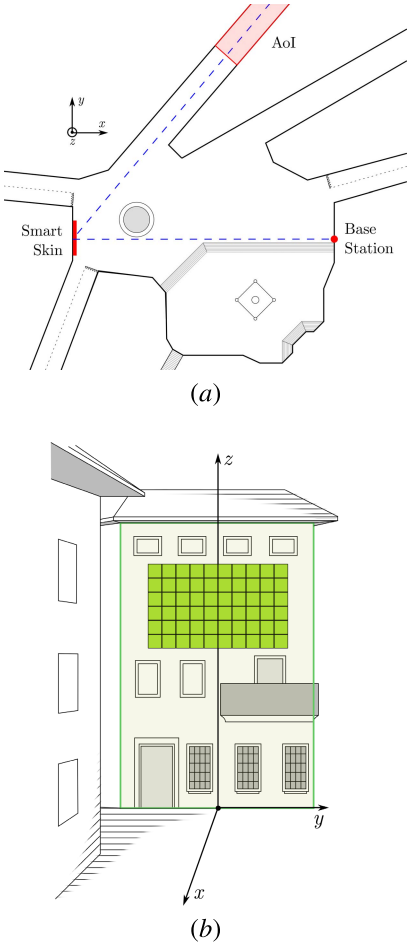

Fig. 4. *Numerical validation—simple skin layout—orthogonal incidence:* $f = 27$ [GHz], $\mathcal{S} = 15$ [m^2], $L = 0.5$ [m], $N = 60$, $\Delta\Omega = 500$ [m^2], and $\mathcal{P}_{th} = -70$ [dB]. Sketch of (a) scenario and (b) admissible surface $\mathcal{S}$ along with its tile discretization.

not affected by the polarization loss [31]. Albeit the presence of undesired sidelobes that are generally unavoidable when dealing with a real implementation of a low-cost artificial metasurface due to the differences between the ideal phase distribution of the theoretical model (2) and the actual one implemented in HFSS [see Fig. 3(a)], the main lobes have a similar shape in both cases, and they are steered toward the same desired angular direction [see Fig. 3(b) and (c)]. Since the pattern generated from the ideal tile according to (2) is free of undesired sidelobes and polarization losses, it seems reasonable to infer that the modular EMSs synthesized in this work will represent reference ideal solutions. From an operative viewpoint, this means that the number M of tiles composing the synthesized EMS layout has to be considered as a lower bound (i.e., the minimum number of tiles for approximating a project target) to be probably increased when going to the implementation of the EMS in a real scenario.

Moving to the design of modular reflecting EMSs for an enhanced wireless coverage, the first test case (*simple skin layout—orthogonal incidence*) refers to the urban scenario depicted in Fig. 4(a), where the BS is located at $\mathbf{r}_{BS}$ with Cartesian coordinates $(x_{BS}, y_{BS}, z_{BS}) = (100, 0, 10)$ [m]. The

TABLE I

Numerical Validation. STATISTICS OF THE REFLECTED POWER $\mathcal{P}_{\Re}(\mathbf{r})$ WITHIN THE AOI, Ω

	$\min_{\mathbf{r}\in\Omega}\left\{\lvert E_{rx}(\mathbf{r})\rvert^2\right\}$ [dB]	$\max_{\mathbf{r}\in\Omega}\left\{\lvert E_{rx}(\mathbf{r})\rvert^2\right\}$ [dB]	$\text{avg}_{\mathbf{r}\in\Omega}\left\{\lvert E_{rx}(\mathbf{r})\rvert^2\right\} = \Phi_1$ [dB]
Fig. 6(*c*)	−69.9	−63.0	−66.8
Fig. 7(*e*)	−173.9	−78.1	−84.7
Fig. 7(*f*)	−90.9	−71.7	−75.0
Fig. 9(*c*)	−69.9	−63.2	−66.9
Fig. 12(*g*)	−69.7	−62.5	−65.1
Fig. 12(*h*)	−69.7	−61.2	−64.4
Fig. 12(*i*)	−101.5	−60.3	−65.1
Fig. 14(*c*)	−73.1	−60.1	−63.5

height of the BS from the ground (i.e., $z_{BS} = 10$ [m]) has been set according to the 3rd Generation Partnership Project (3GPP) guidelines for the *urban-micro* (UMi) cell scenario [32]. Moreover, the BS has been assumed to radiate a plane wave at $f = 27$ [GHz] having the electric field vertically polarized ($\widehat{\mathbf{e}}_r = \widehat{\mathbf{z}}$) with unitary amplitude $E_{\Im} = 1.0$ [V/m] that impinges from the ϕ-normal direction ($\phi_{\Im}^{(0)} = 0.0$ [deg]) on the EMS placed on the yz plane [i.e., $x_{\mathcal{S}}^{(n)} = 0$ $(n = 1, \ldots, N)$] [see Fig. 4(b)] at a distance of $d_{\Im}^{(0)} = 100$ [m] from the BS. The admissible surface $\mathcal{S}$ for the deployment of the artificial EMS on the building facade [see Fig. 4(b)] has been chosen with an area $\Delta\mathcal{S} = 15$ [m^2], and it extends within the range -2.5 [m] $\leq y_{\mathcal{S}} \leq 2.5$ [m] and 5.0 [m] $\leq z_{\mathcal{S}} \leq 8.0$ [m] along the y-axis and the z-axis, respectively. Such an area $\mathcal{S}$ has been partitioned into $N = 60$ square subdomains of size $\Delta\mathcal{S}^{(n)} = L^{(n)} \times L^{(n)}$ $(n = 1, \ldots, N)$ being $L^{(n)} = 0.5$ [m] so that there are $N_y = 10$ and $N_z = 6$ partitions along the y-axis and the z-axis, respectively (i.e., $N = N_y \times N_z$). By enumerating the admissible locations of the EMS tiles in a raster scan way, starting from the top left corner of $\mathcal{S}$, the barycenter of the nth $(n = 1, \ldots, N)$ subdomain of $\mathcal{S}$ has the following coordinates:

$$y_{\mathcal{S}}^{(n)} = y_{\mathcal{S}}^{(1)} + \left(n - 1 - \left\lfloor \frac{n-1}{N_y} \right\rfloor N_y\right) \times L^{(n)}$$
$$z_{\mathcal{S}}^{(n)} = z_{\mathcal{S}}^{(1)} - \left\lfloor \frac{n-1}{N_y} \right\rfloor \times L^{(n)} \tag{6}$$

$(n = 2, \ldots, N)$, with $y_{\mathcal{S}}^{(1)} = -2.25$ [m] and $z_{\mathcal{S}}^{(1)} = 7.75$ [m] being the coordinates of the barycenter of the first $(n = 1)$ location admissible for a tile.

The goal of the EMS design is that of enhancing the power strength in the AoI Ω of size $\Delta\Omega = 10 \times 50$ [m^2] located in $x_{\Omega}^{(0)} = 80.35$ [m] and $y_{\Omega}^{(0)} = 95.75$ [m] [see Fig. 4(a)] along the azimuth direction $\phi_{\Re}^{(0)} = 50.0$ [deg] with respect to the EMS, with $\mathcal{P}_{th} = -70$ [dB] being the threshold on the desired coverage in (4), while the "no connection" power level has been set to $\mathcal{P}_{bls} \approx -100$ [dB]. In order to assess the "coverage" condition within the AoI, $U = 500$ ideal receivers have been uniformly distributed within Ω, that is, one receiver every $\Delta\Omega = 1$ [m^2], at the height $z_u = 1.5$ [m] to emulate users on the ground [32].

Concerning the NSGA-II algorithm, the following setup of the control parameters has been used: $P = 2 \times N$, $I = 1000$, $\wp_c = 1.0$, $\wp_m = 1/N$, $\aleph_c = 15$, and $\aleph_m = 20$. Moreover, each

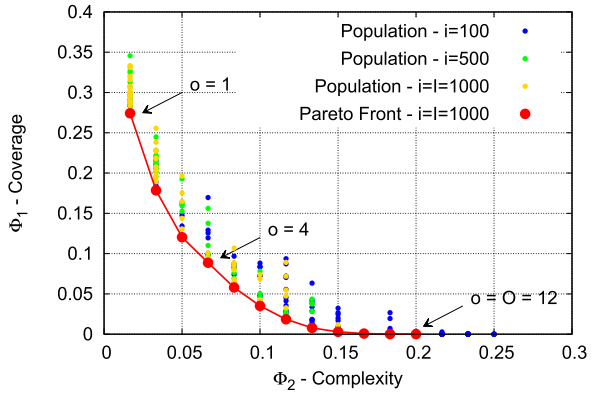

Fig. 5. *Numerical validation—simple skin layout—orthogonal incidence:* $f = 27$ [GHz], $\mathcal{S} = 15$ [m^2], $L = 0.5$ [m], $N = 60$, $\Delta\Omega = 500$ [m^2], and $\mathcal{P}_{th} = -70$ [dB]. Iterative ($i = 100$, $i = 500$, and $i = I$) evolution of the population of the P ($P = 2 \times N$) trial solutions $\{\mathbf{T}_i^{(p)}; p = 1, \ldots, P\}$ in the space of the design objectives and Pareto front at convergence ($i = I$) $\{\mathbf{T}_{opt}^{(o)}; o = 1, \ldots, O\}$.

simulation has been repeated 50 times with different random seeds to statistically validate the results from the stochastic optimization. However, since all simulations led to similar Pareto fronts at convergence ($i = I$), only the solutions of a representative run will be reported and discussed in the following.

Fig. 5 shows the population of trial solutions, $\{\mathbf{T}_i^{(p)}; p = 1, \ldots, P\}$, at the iterations $i = 100$, $i = 500$, and $i = I$ in the space of the objectives along with the Pareto front of $O = 12$ nondominated solutions at the convergence ($i = I$), $\{\mathbf{T}_{opt}^{(o)}; o = 1, \ldots, O\}$. Let us now analyze the EMS solution that fully fits the coverage requirements [i.e., $\Phi_1(\mathbf{T}_{opt}^{(o)}) = 0$], which corresponds to the Oth representative point of the Pareto front, whose chromosome has $M = 12$ bits at one (i.e., $t_{n,opt}^{(o)}\rfloor_{o=12} = 1$, and $n = \{3, 4, 5, 6, 8, 12, 30, 32, 43, 44, 45, 46\}$) so that the EMS layout turns out being composed by $M = 12$ tiles, as shown in Fig. 6(a). The support of such an EMS amounts to $\Delta\mathcal{S}_{opt}^{(o)}\rfloor_{o=12} = 3$ [m^2], which is one fifth of the whole admissible EMS surface (i.e., $((\Delta\mathcal{S}_{opt}^{(o)}\rfloor_{o=12})/(\Delta\mathcal{S})) = 20\%$). The coverage improvement enabled by the installation of such an artificial skin on the building facade is pointed out in Fig. 6(b) where the map of the reflected power $\mathcal{P}_{\Re}(\mathbf{r})$ at $z = 1.5$ [m] from the ground is shown in a region Ψ, around the AoI, of extension $\Delta\Psi = 200 \times 200$ [m^2]. As it can be observed, the power intensity along the direction of the street passing through

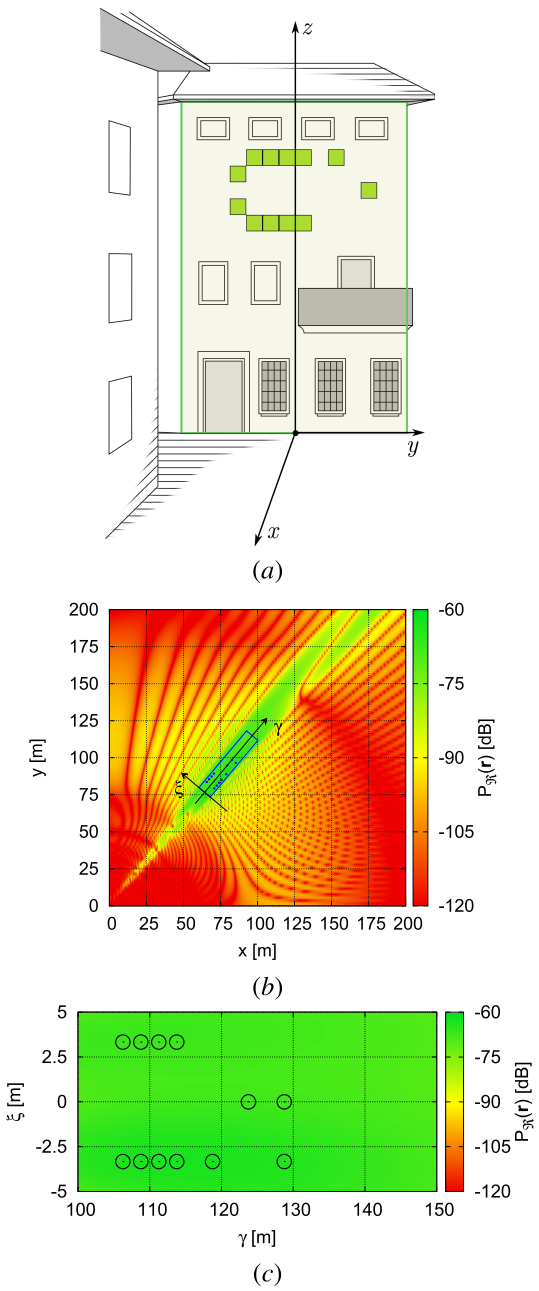

Fig. 6. *Numerical validation—simple skin layout—orthogonal incidence:* $f = 27$ [GHz], $\mathcal{S} = 15$ [m^2], $L = 0.5$ [m], $N = 60$, $\Delta\Omega = 500$ [m^2], and $\mathcal{P}_{th} = -70$ [dB]. Plot of (a) EMS layout of the Oth ($O = 12$) solution, $\mathcal{S}_{opt}^{(O)}$, of the Pareto front in Fig. 5 and map of the spatial distribution of the power, $\mathcal{P}_{\Re}(\mathbf{r})$, reflected from the EMS in (b) region Ψ and within (c) AoI Ω ($\Omega \subset \Psi$).

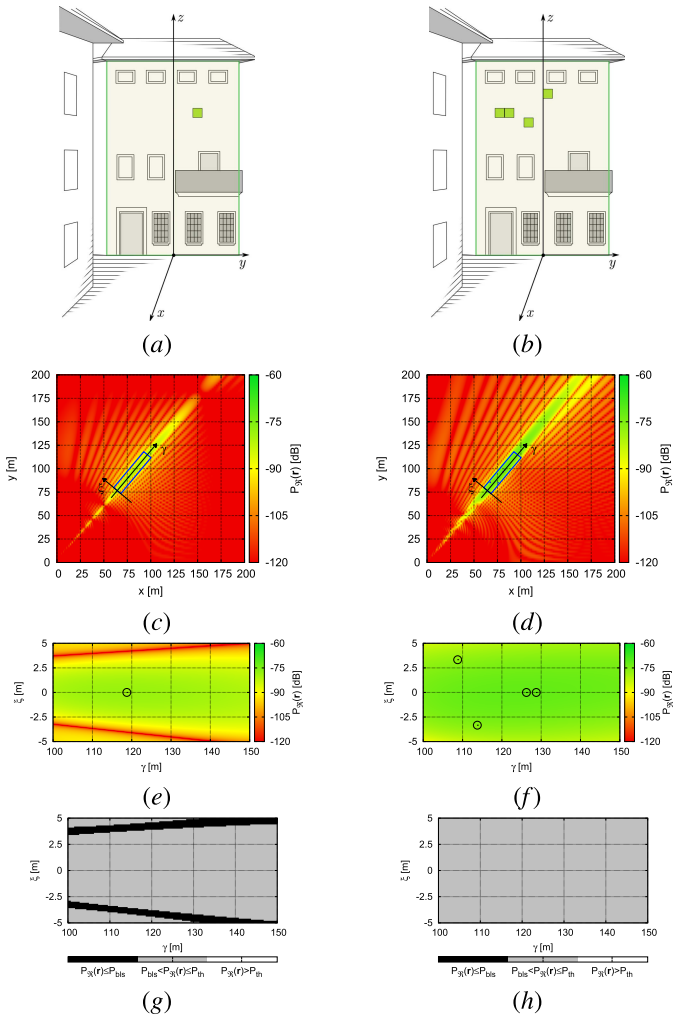

Fig. 7. *Numerical validation—simple skin layout—orthogonal incidence:* $f = 27$ [GHz], $\mathcal{S} = 15$ [m^2], $L = 0.5$ [m], $N = 60$, $\Delta\Omega = 500$ [m^2], $\mathcal{P}_{th} = -70$ [dB], and $\mathcal{P}_{bls} \approx -100$ [dB]. Plots of (a) and (b) EMS layout and (c)–(f) corresponding spatial distributions of the power, $\mathcal{P}_{\Re}(\mathbf{r})$, reflected from the EMS along with (g) and (h) coverage/connectivity maps for (a), (c), (e), and (g) $o = 1$ and (b), (d), (f), and (h) $o = 4$ solutions of the Pareto front in Fig. 5.

Ω has been significantly increased. As a matter of fact, the signal turns out to be stronger not only in Ω but also before and after [see Fig. 6(b)] since the skin tiles generate simple pencil beams (2) with an elongated footprint on the ground, the dots in Fig. 6(b) and (c) being the $M = 12$ points $\mathbf{r}_{\Omega}^{(n)}$ and $n = \{3, 4, 5, 6, 8, 12, 30, 32, 43, 44, 45, 46\}$, where the peaks of the beams reflected from the M EMS tiles are directed. Regardless of the simplicity of the beam afforded by a single EMS tile, the combined use of multiple/modular tiles has allowed to reach the desired average power threshold $\mathcal{P}_{th} = -70$ [dB] (i.e., $\Phi_1(\mathbf{T}_{opt}^{(o)}\rfloor_{o=12}) = 0$) in the whole AoI, as shown in Fig. 6(c), with $\gamma - \xi$ being the Ω local coordinate system [see Fig. 6(b)]. Indeed, the statistics of the power reflected in Ω are $\min_{\mathbf{r}\in\Omega}\{\mathcal{P}_{\Re}(\mathbf{r}_u; \mathbf{T}_{opt}^{(o)}\rfloor_{o=12})\} = -69.9$ [dB], $\max_{\mathbf{r}\in\Omega}\{\mathcal{P}_{\Re}(\mathbf{r}_u; \mathbf{T}_{opt}^{(o)}\rfloor_{o=12})\} = -63.0$ [dB], and $\text{avg}_{\mathbf{r}\in\Omega}\{\mathcal{P}_{\Re}(\mathbf{r}_u; \mathbf{T}_{opt}^{(o)}\rfloor_{o=12})\} = -66.8$ [dB], respectively (see Table I).

For the sake of completeness, other two representative solutions of the Pareto front in Fig. 5 are analyzed. The EMS layouts and the maps of the power reflected in Ψ of the solution with minimum complexity ($o = 1$—Fig. 5) and the one having $\Phi_1(\mathbf{T}_{opt}^{(o)})\rfloor_{o=4} \approx 0.1$ (i.e., $\text{avg}_{\mathbf{r}\in\Omega}\{\mathcal{P}_{\Re}(\mathbf{r}_u; \mathbf{T}_{opt}^{(o)}\rfloor_{o=12})\} = -77$ [dB]) are reported in Fig. 7.

The minimum complexity EMS (i.e., $\Phi_2(\mathbf{T}_{opt}^{(o)}\rfloor_{o=1}) = 1/60$) needs only one ($M = 1$) tile [see Fig. 7(a)], but the average power level in Ω reduces of $\delta\Phi_1]_{o=1}^{o=12} = 17.9$ [dB] ($\delta\Phi]_{o'}^{o} \triangleq \Phi(\mathbf{T}_{opt}^{(o)}) - \Phi(\mathbf{T}_{opt}^{(o')})$; $o, o' \in [1, O]$) with respect to that in

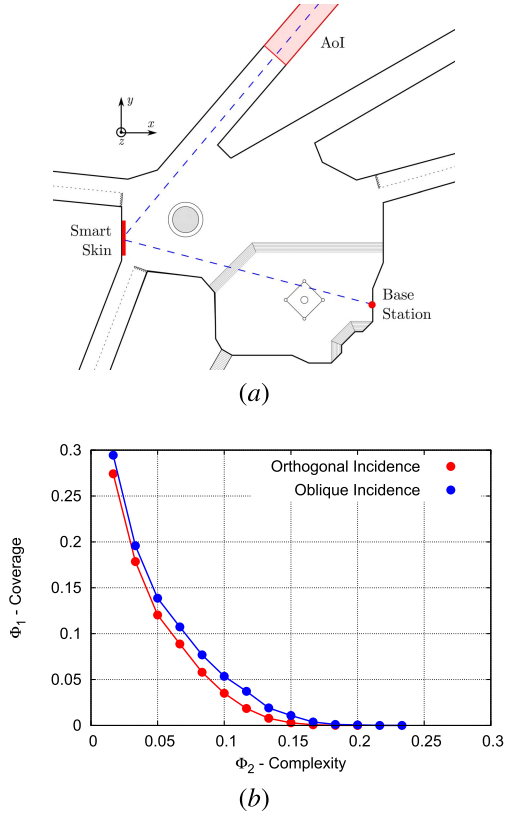

Fig. 8. *Numerical validation—simple skin layout—oblique incidence:* $f = 27$ [GHz], $\mathcal{S} = 15$ [m^2], $L = 0.5$ [m], $N = 60$, $\Delta\Omega = 500$ [m^2], and $\mathcal{P}_{th} = -70$ [dB]. Sketch of (a) scenario and plot of (b) Pareto front at convergence $(i = I)$ $\{\mathbf{T}_{opt}^{(o)}; o = 1, \ldots, O\}$.

Fig. 6(a). Due to the presence of a single tile, the map of the EM power in Fig. 7(c) shows the classical footprint of a pencil beam characterized by a mainlobe focused in the point $\mathbf{r}_{\Omega}^{(n)}\rfloor_{n=28}$ within Ω [see Fig. 7(c)] along the central line of the AoI ($\xi = 0$) [see Fig. 7(e)], while there are portions of Ω close to $\xi = \pm 5$ [m] where the power strength is very low [see Fig. 7(e)]. Quantitatively, it turns out that the condition $\mathcal{P}_{th} \leq \mathcal{P}_{\Re}(\mathbf{r}_u; \mathbf{T}_{opt}^{(o)}\rfloor_{o=1})$ never holds true [see Fig. 7(e)] since also the power peak is below the desired QoS threshold ($\mathcal{P}_{\Re}(\mathbf{r}_u; \mathbf{T}_{opt}^{(o)}\rfloor_{o=1}) = -78.1$ [dB]). Moreover, the minimum level of the power reflected within the AoI by such a single-tile EMS of side $L^{(1)} = 0.5$ [m] is equal to $\min_{\mathbf{r}\in\Omega}\{\mathcal{P}_{\Re}(\mathbf{r}_u; \mathbf{T}_{opt}^{(o)}\rfloor_{o=1})\} = -173.9$ [dB] (see Table I), which is (well) below the "connectivity" threshold of $\mathcal{P}_{bls} = -100$ [dB]. Such an undesired condition verifies in other portions of Ω where there is not enough signal for assuring the users' connections [$\mathcal{P}_{\Re}(\mathbf{r}_u; \mathbf{T}_{opt}^{(o)}\rfloor_{o=1}) < \mathcal{P}_{bls}$—Fig. 7(g)].

By using three more tiles [i.e., $M = 4$—Fig. 7(b)], the power level reflected on Ω turns out significantly higher [see Fig. 7(d)], with the average power being increased of almost ten times (i.e., $\delta\Phi_1]_{o=1}^{o=4} = 9.7$ [dB]), and there are no more "no connection" zones within Ω [see Fig. 7(h)] since $\min_{\mathbf{r}\in\Omega}\{\mathcal{P}_{\Re}(\mathbf{r}_u; \mathbf{T}_{opt}^{(o)}\rfloor_{o=4})\} = -90.9$ [dB] (see Table I), even though the power peak is still slightly lower than the QoS threshold ($\max_{\mathbf{r}\in\Omega}\{\mathcal{P}_{\Re}(\mathbf{r}_u; \mathbf{T}_{opt}^{(o)}\rfloor_{o=4})\} = -71.7$ [dB]).

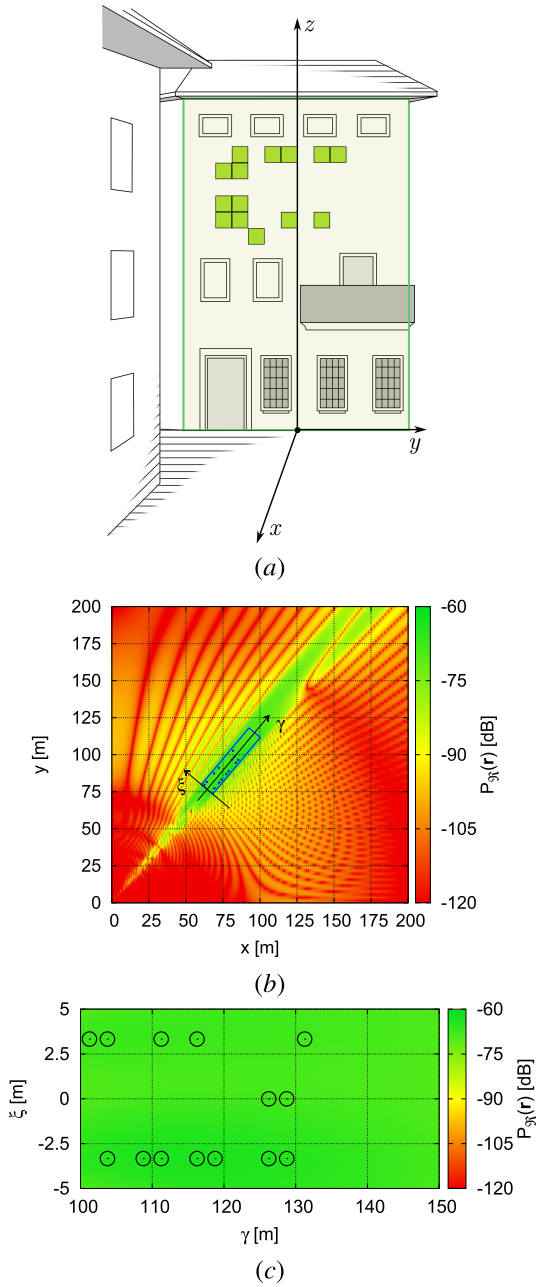

Fig. 9. *Numerical validation—simple skin layout—oblique incidence:* $f = 27$ [GHz], $\mathcal{S} = 15$ [m^2], $L = 0.5$ [m], $N = 60$, $\Delta\Omega = 500$ [m^2], and $\mathcal{P}_{th} = -70$ [dB]. Plot of (a) EMS layout of the Oth ($O = 14$) solution, $\mathcal{S}_{opt}^{(O)}$, of the Pareto front in Fig. 5 and map of the spatial distribution of the power, $\mathcal{P}_{\Re}(\mathbf{r})$, reflected from the EMS in (b) region Ψ and within (c) AoI Ω ($\Omega \subset \Psi$).

In the second test case (*simple skin layout—oblique incidence*), the field generated from the BS has been assumed impinging on the EMS with an oblique incidence on the azimuth plane (i.e., $\phi_{\Im}^{(0)} = 20$ [deg]), with being $(x_{BS}, y_{BS}, z_{BS}) = (93.9, 34.2, 10)$ [m] such that $d_{\Im}^{(0)} = 100$ [m] as in the previous example [see Fig. 8(a)]. All other features concerned with the EM field generated from the BS (i.e., frequency and polarization), the area and the discretization of $\mathcal{S}$, and the coverage area under analysis Ω have been kept unaltered from the first test case.

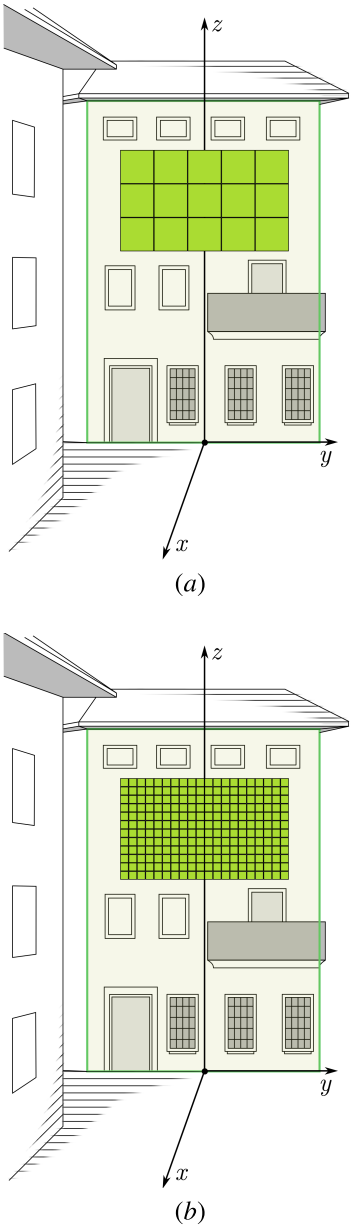

Fig. 10. *Numerical validation—simple skin layout—varying tiles size:* $f = 27$ [GHz], $\mathcal{S} = 15$ [m^2], $N = \{240, 15\}$, and $\mathcal{P}_{th} = -70$ [dB]. Sketches of the scenario and of the admissible surface $\mathcal{S}$ along with its discretization when using tiles with side lengths (a) $L = 1.0$ [m] and (b) $L = 0.25$ [m].

The Pareto front of the O optimal tradeoff solutions determined by the proposed NSGA-II-based approach is compared in Fig. 8(b) with that obtained in the "normal incidence" case (see Fig. 5). The reader can observe that the Pareto front of the "oblique incidence" scenario consists of $O = 14$ EMS designs (versus $O = 12$—"normal incidence"), and it turns out that the oblique incidence from the BS needs a higher number of tiles to yield the same coverage of the "normal incidence" solutions [see Fig. 8(b)]. As expected, a wider area is now required because of the reduction of the effective area of the EMS (2) since a lower amount of power is intercepted from the incident wave with the same area of the "normal incidence" EMS.

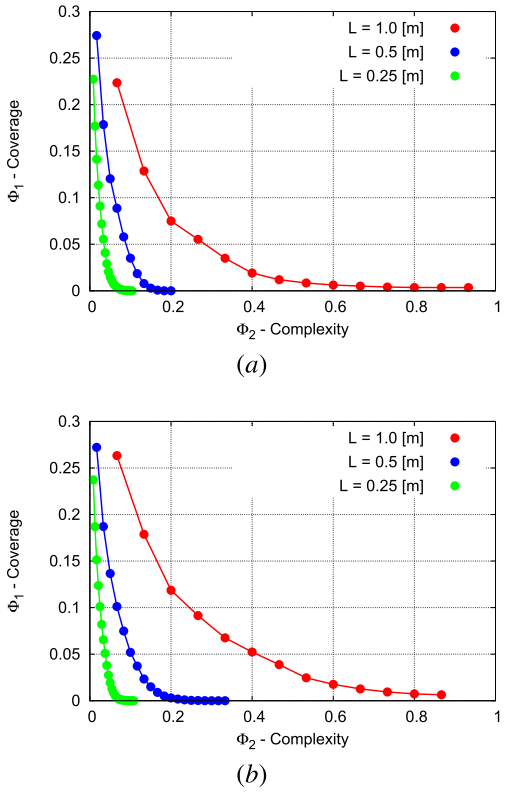

Fig. 11. *Numerical validation—simple skin layout—varying tiles size:* $f = 27$ [GHz], $\mathcal{S} = 15$ [m^2], and $\mathcal{P}_{th} = -70$ [dB]. Plot of the Pareto fronts at convergence ($i = I$) $\{\mathbf{T}_{opt}^{(o)}; o = 1, \ldots, O\}$ for different square tile sizes (L being the side length of the tile) in correspondence with an AoI Ω of dimension: (a) $\Delta\Omega = 10 \times 50 = 500$ [m^2] and (b) $\Delta\Omega = 10 \times 100 = 1000$ [m^2].

Fig. 9 summarizes the characteristics of the Oth ($O = 14$) solution that fits the coverage requirement [i.e., $\mathcal{P}_{\Re}(\mathbf{r}_u; \mathbf{T}_{opt}^{(O)}) \geq \mathcal{P}_{th} \rightarrow \Phi_1(\mathbf{T}_{opt}^{(O)}) = 0$]. More in detail, the layout of the corresponding EMS is composed by $M = 14$ tiles [see Fig. 9(a)], that is, two more than those of the Oth EMS for the normal incidence, and the arising tiles arrangement is also quite different [see Fig. 9(a) versus Fig. 6(a)]. On the contrary, the power distributions are quite similar as pictorially shown by comparison of the maps in Fig. 9(b) and (c) with those in Fig. 6(b) and (c) and also confirmed by the statistics of the power reflected by the EMS within the AoI (see Table I). Indeed, the differences among the values of the statistical indices are null or negligible (i.e., $\delta\mathcal{P}_{\Re}^{min}]_{Normal}^{Oblique} = 0.0$ [dB], $\delta\mathcal{P}_{\Re}^{max}]_{Normal}^{Oblique} = 0.2$ [dB], and $\delta\mathcal{P}_{\Re}^{av}]_{Normal}^{Oblique} = \delta\Phi_1]_{Normal}^{Oblique} = -0.1$ [dB], being $\delta\mathcal{P}_{\Re}^{stat}]_{Normal}^{Oblique} \triangleq \text{stat}_{\mathbf{r}\in\Omega}\{\mathcal{P}_{\Re}(\mathbf{r}_u; \mathbf{T}_{opt}^{(o)}\rfloor_{o=O}^{Oblique})\} - \text{stat}_{\mathbf{r}\in\Omega}\{\mathcal{P}_{\Re}(\mathbf{r}_u; \mathbf{T}_{opt}^{(o)}\rfloor_{o=O}^{Normal})\}$—Table I).

The third design experiment (*simple skin layout—varying tiles size*) is concerned with a surface $\mathcal{S}$ still discretized with uniform tiles but considering different tile sizes: $L^{(n)} = 1.0$ [m] [$\rightarrow N = N_y \times N_z = 5 \times 3 = 15$—Fig. 10(a)] or $L^{(n)} = 0.25$ [m] [$\rightarrow N = N_y \times N_z = 20 \times 12 = 240$—Fig. 10(b)] ($n = 1, \ldots, N$). In the former case, there are few admissible tiles reflecting a narrow beam toward the AoI, while the number of tiles and DoFs is 16 times larger in the latter

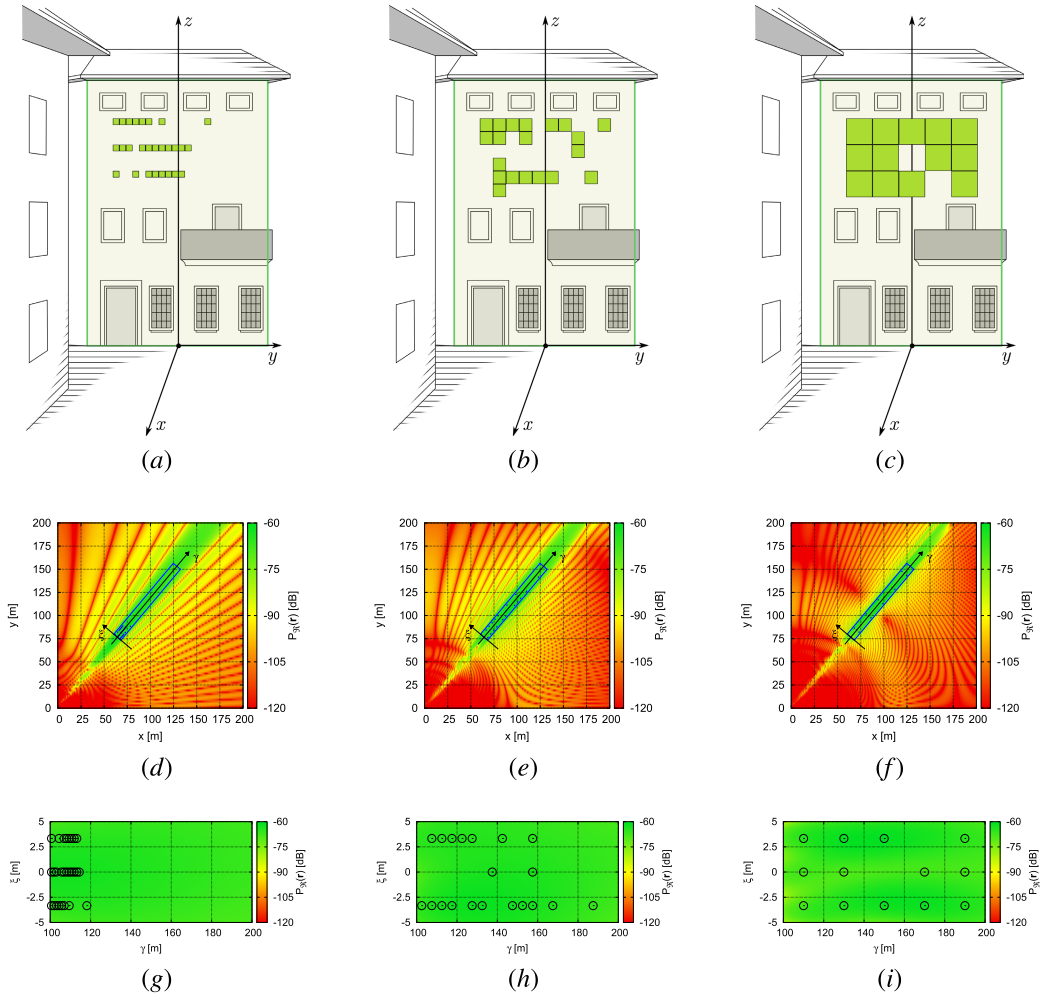

Fig. 12. *Numerical validation—simple skin layout—varying tiles size:* $f = 27$ [GHz], $\mathcal{S} = 15$ [m^2], $L = \{0.25, 0.5, 1.0\}$ [m], $N = \{240, 60, 15\}$, $\Delta\Omega = 1000$ [m^2], and $\mathcal{P}_{th} = -70$ [dB]. Plots of (a)–(c) EMS layouts of the Oth solution, $\mathcal{S}_{opt}^{(O)}$, of the Pareto fronts in Fig. 11(b) and maps of the spatial distribution of the power, $\mathcal{P}_{\Re}(\mathbf{r})$, reflected from the EMS in (d)–(f) region Ψ and within (g)–(i) AoI Ω ($\Omega \subset \Psi$) when using tiles with side length (a), (d), and (g) $L = 0.25$ [m], (b), (e), and (h) $L = 0.25$ [m], and (c), (f), and (i) $L = 1.0$ [m].

case where the beam reflected by each mth ($m = 1, \ldots, M$) installed tile has a broader coverage.

The NSGA-II optimization has been run for both tile sizes, and the Pareto fronts obtained at the convergence ($i = I$) are shown in Fig. 11(a) along with that of Fig. 5, which is related to the tile size $L^{(n)} = 0.5$ [m] ($n = 1, \ldots, N$). The plots in Fig. 11(a) indicate that the wider the tile size, the higher is the value of the complexity index Φ_2 to fulfill (3). Furthermore, it is worth highlighting that, when $L^{(n)} = 1.0$ [m], no solution of the Pareto front satisfies the coverage requirement since $\Phi_1(\mathbf{T}_{opt}^{(O)}) > 0$, while the coverage condition holds true using smaller tiles.

The same conclusions arise when extending the coverage area Ω from $\Delta\Omega = 10 \times 50$ [m^2] [see Fig. 11(a)] up to $\Delta\Omega = 10 \times 100$ [m^2] [see Fig. 11(b)]. For this latter case, the layouts and the coverage maps of the solutions providing the best coverage (i.e., the Oth of the Pareto front) for each tile size are shown in Fig. 12. By analyzing the power distributions in Fig. 12(d)–(f), it turns out that the main advantage of using larger tiles, which reflect narrower beams, is the capability of better focusing the reflected field only along the direction of the AoI [see Fig. 12(f) versus Fig. 12(d)]. This is not for free, and the cost to pay is that of having a very large EMS composed by $M = 13$ tiles, each of $\Delta\mathcal{S}^{(m)} = 1$ [m^2] ($m = 1, \ldots, M$), for a total surface of $\Delta\mathcal{S}_{opt}^{(O)}\rfloor_{L=1.0\ [\mathrm{m}]} = 13$ [m^2], while the area occupied by the EMS when using square tiles of size $L^{(n)} = 0.25$ [m] [see Fig. 12(a)] and $L^{(n)} = 0.5$ [m] [see Fig. 12(b)] amounts to $\Delta\mathcal{S}_{opt}^{(O)}\rfloor_{L=0.25\ [\mathrm{m}]} \simeq 1.69$ [m^2] and $\Delta\mathcal{S}_{opt}^{(O)}\rfloor_{L=0.5\ [\mathrm{m}]} = 5$ [m^2], respectively. This means that the limited focusing capability of smaller tiles is balanced by a reduction of the required EMS extension, thus a lower cost of the EMS.

In the last design example (*complex skin layout—orthogonal incidence*), the admissible region $\mathcal{S}$ on the building facade is more complex [see Fig. 13(a)] since the area dedicated to the EMS deployment is smaller, and there are more architectural constraints (e.g., misaligned windows and open window shutters) as in historical buildings. As for the descriptive parameters of the scenario at hand, they have been defined as in the "*simple skin layout—orthogonal incidence*"

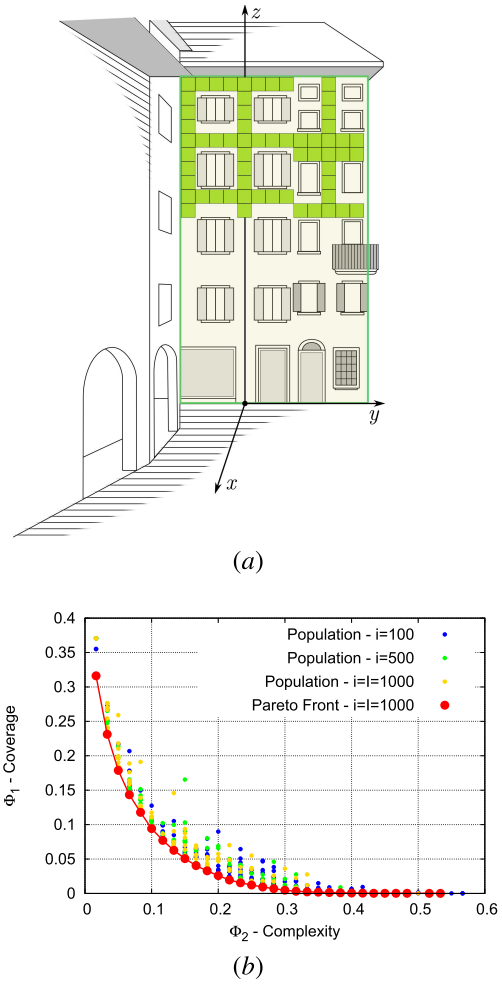

Fig. 13. *Numerical validation—complex skin layout—orthogonal incidence:* $f = 27$ [GHz], $\mathcal{S} = 15$ [m^2], $L = 0.5$ [m], $N = 60$, $\Delta\Omega = 1000$ [m^2], and $\mathcal{P}_{th} = -70$ [dB]. Sketch of (a) scenario and of the admissible surface $\mathcal{S}$ along with its tile discretization and the plot of (b) iterative ($i = 100$, $i = 500$, and $i = I$) evolution of the population of the P ($P = 2 \times N$) trial solutions $\{\mathbf{T}_i^{(p)}; p = 1, \ldots, P\}$ in the space of the design objectives along with the Pareto front at convergence ($i = I$) $\{\mathbf{T}_{opt}^{(o)}; o = 1, \ldots, O\}$.

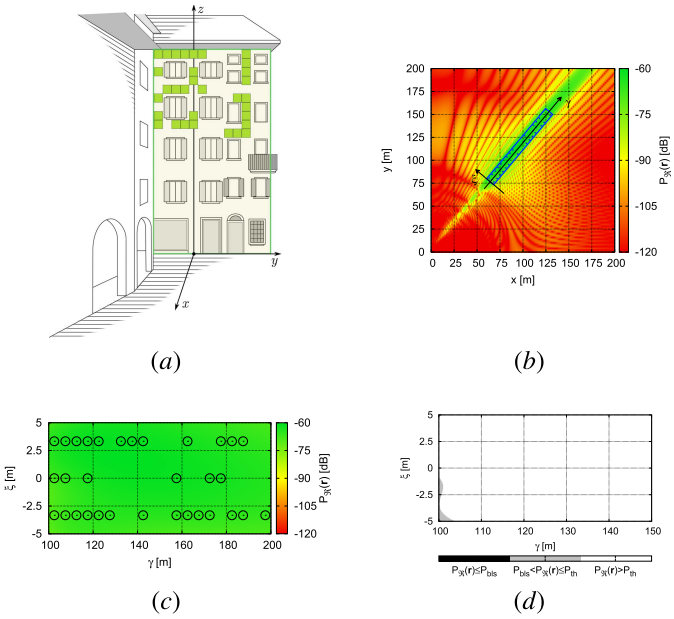

Fig. 14. *Numerical validation—complex skin layout—orthogonal incidence:* $f = 27$ [GHz], $\mathcal{S} = 15$ [m^2], $L = 0.5$ [m], $N = 60$, $\Delta\Omega = 1000$ [m^2], and $\mathcal{P}_{th} = -70$ [dB]. Plot of (a) EMS layout and of (b), and (c) corresponding spatial distributions of the power, $\mathcal{P}_{\Re}(\mathbf{r})$, reflected from the EMS along with (d) coverage/connectivity maps for the Oth ($O = 31$) solution of the Pareto front in Fig. 13(b).

case, but a larger AoI (i.e., $\Delta\Omega = 10 \times 100$ [m^2]) has been considered.

The evolution ($i = 100$, $i = 500$, and $i = I$) of the population of EMS trial solutions, $\{\mathbf{T}_i^{(p)}; p = 1, \ldots, P\}$, in the space of the objectives is shown in Fig. 13(b) together with the Pareto front at convergence ($i = I$), which includes $O = 31$ nondominated solutions $\{\mathbf{T}_{opt}^{(o)}; o = 1, \ldots, O\}$. As it can be noticed [see Fig. 13(b)], 15 EMS of the Pareto front have values of the coverage index smaller than $\Phi_1(\mathbf{T}_{opt}^{(o)}\rfloor_o) < 10^{-2}$.

The Oth solution, which fully satisfies the coverage requirements, is done by $M = 32$ tiles of size $\Delta\mathcal{S}^{(m)} = 0.5 \times 0.5$ [m^2] ($m = 1, \ldots, M$), and it covers a surface area of $\Delta\mathcal{S}_{opt}^{(O)} = 8$ [m^2] [see Fig. 14(a)]. Despite the irregularity of the EMS layout, the coverage maps in Fig. 14(b)–(d) confirm that the proposed EMS design method properly selects, from the admissible pool, a subset of tiles that guarantees the required power level within the AoI Ω (see Table I).

V. Conclusion

Within the SEME vision, this article has proposed a novel strategy to improve the signal strength in urban areas where the power radiated by the BS is too strongly attenuated. More specifically, such an approach proposes the use of modular, passive, and static artificial metasurfaces to be installed/embedded on the facades of urban buildings, such as coating skins, to enhance the coverage by reflecting the EM wave coming from the BS toward the desired directions within an AoI. In order to fulfill user-defined coverage conditions, while minimizing the cost/complexity, the design of the EMS has been cast as a multiobjective optimization problem, and it has been addressed by means of a binary implementation of the NSGA-II algorithm.

From a technological and methodological viewpoint, the main novelties, to the best of our knowledge, of this research work can be summarized as follows.:

1) the introduction for the first time of a novel cost-effective solution, to be possibly implemented through cheap printed technology, for the large-scale deployment of artificial metasurfaces to be installed on the facades of buildings for improving the wireless coverage in urban scenarios;
2) the suitability of the proposed technological solution in future wireless networks due to its "green" (i.e., passive) and noninvasive (i.e., low profile and without heavy architectural impact) nature;
3) the development of a customized design strategy to enable an effective/efficient optimization-based design of (also large) EMSs composed of simple (also nonhomogeneous) tiles.

From the numerical assessment, which has been carried out by considering realistic topological urban scenarios and a millimeter-wave 5G frequency band, the following outcomes can be drawn.

1) The use of tiled EMSs always improves the coverage of the AoI.
2) The NSGA-II-based synthesis approach provides the designer with a Pareto front of multiple EMS solutions, which are tradeoffs between coverage requirements and complexity of the EMS layout. In all the considered scenarios, an EMS that fulfills the user-defined coverage condition (i.e., not only the user connection) has been (generally) found without using the whole area available on the facade of the building.
3) The number and the positions of the tiles of the EMS layout depend on the relative position between the BS and the AoI. Moreover, the dimension (e.g., small, medium, and large) and the distribution (e.g., uniform or nonuniform) of the tiles composing the EMS are other DoFs, which can be exploited to fit the coverage conditions and other architectural constraints (e.g., misaligned windows and open window shutters).

Future research activities, beyond the scope of this article, will integrate the design of the tiles' layouts within the proposed iterative optimization loop in order to take into account nonideal reflections and polarization losses, and the possibility to design more complex (e.g., conformal and not flat) skin surfaces. Moreover, the presence of multiple BSs and AoIs will be dealt with toward the definition of a tool for network planning, and the use of such skins will be also investigated for improving the coverage indoors.

ACKNOWLEDGMENT

Andrea Massa wishes to thank E. Vico for her never-ending inspiration, support, guidance, and help.

REFERENCES

[1] R. L. Haupt, *Wireless Communications Systems: An Introduction*. Hoboken, NJ, USA: Wiley, 2020.

[2] J. Korhonen, *Introduction to 4G Mobile Communications*. Boston, MA, USA: Artech House, 2014.

[3] C. Cox, *An Introduction to 5G: The New Radio, 5G Network and Beyond*. Hoboken, NJ, USA: Wiley, 2021.

[4] K. Yu, L. Lin, M. Alazab, L. Tan, and B. Gu, "Deep learning-based traffic safety solution for a mixture of autonomous and manual vehicles in a 5G-enabled intelligent transportation system," *IEEE Trans. Intell. Transp. Syst.*, vol. 22, no. 7, pp. 4337–4347, Jul. 2021.

[5] C. Li *et al.*, "5G-based systems design for tactile internet," *Proc. IEEE*, vol. 107, no. 2, pp. 307–324, Feb. 2019.

[6] A. Acemoglu *et al.*, "5G robotic telesurgery: Remote transoral laser microsurgeries on a cadaver," *IEEE Trans. Med. Robot. Bionics*, vol. 2, no. 4, pp. 511–518, Nov. 2020.

[7] M. Bennis, M. Debbah, and H. V. Poor, "Ultrareliable and low-latency wireless communication: Tail, risk, and scale," *Proc. IEEE*, vol. 106, no. 10, pp. 1834–1853, Oct. 2018.

[8] M. Wang, F. Gao, S. Jin, and H. Lin, "An overview of enhanced massive MIMO with array signal processing techniques," *IEEE J. Sel. Topics Signal Process.*, vol. 13, no. 5, pp. 886–901, Sep. 2019.

[9] A. Puglielli *et al.*, "Design of energy- and cost-efficient massive MIMO arrays," *Proc. IEEE*, vol. 104, no. 3, pp. 586–606, Mar. 2016.

[10] W. Hong *et al.*, "The role of millimeter-wave technologies in 5G/6G wireless communications," *IEEE J. Microw.*, vol. 1, no. 1, pp. 101–122, Jan. 2021.

[11] F. Yang, D. Erricolo, and A. Massa, "Special issue on smart electromagnetic environment," *IEEE Trans. Antennas Propag.*, vol. 69, no. 3, p. 1838, Mar. 2021.

[12] M. Salucci, B. Li, A. Benoni, P. Rocca, and A. Massa, "Smart EM environment as enabling technology for future wireless systems," in *Proc. 14th Int. Congr. Artif. Mater. Novel Wave Phenomena (Metamaterials)*, New York, NY, USA, Sep./Oct. 2020, pp. 48–50.

[13] F. Yang and Y. Rahmat-Samii, *Surface Electromagnetics: With Applications in Antenna, Microwave, and Optical Engineering*. Cambridge, U.K.: Cambridge Univ. Press, 2019.

[14] M. Di Renzo *et al.*, "Smart radio environments empowered by reconfigurable AI meta-surfaces: An idea whose time has come," *EURASIP J. Wireless Commun. Netw.*, vol. 2019, no. 1, pp. 1–20, 2019.

[15] E. Basar, M. Di Renzo, J. De Rosny, M. Debbah, M. Alouini, and R. Zhang, "Wireless communications through reconfigurable intelligent surfaces," *IEEE Access*, vol. 7, pp. 116753–116773, 2019.

[16] M. Di Renzo *et al.*, "Smart radio environments empowered by reconfigurable intelligent surfaces: How it works, state of research, and the road ahead," *IEEE J. Sel. Areas Commun.*, vol. 38, no. 11, pp. 2450–2525, Nov. 2020.

[17] J. A. Hodge, K. V. Mishra, and A. I. Zaghloul, "Intelligent time-varying metasurface transceiver for index modulation in 6G wireless networks," *IEEE Antennas Wireless Propag. Lett.*, vol. 19, no. 11, pp. 1891–1895, Nov. 2020.

[18] B. G. Kashyap, P. C. Theofanopoulos, Y. Cui, and G. C. Trichopoulos, "Mitigating quantization lobes in mmWave low-bit reconfigurable reflective surfaces," *IEEE Open J. Antennas Propag.*, vol. 1, pp. 604–614, 2020.

[19] A. Pitilakis *et al.*, "A multi-functional reconfigurable metasurface: Electromagnetic design accounting for fabrication aspects," *IEEE Trans. Antennas Propag.*, vol. 69, no. 3, pp. 1440–1454, Mar. 2021.

[20] Q. Wu, S. Zhang, B. Zheng, C. You, and R. Zhang, "Intelligent reflecting surface-aided wireless communications: A tutorial," *IEEE Trans. Commun.*, vol. 69, no. 5, pp. 3313–3351, May 2021.

[21] M. Wang, S. Xu, F. Yang, and M. Li, "A 1-bit bidirectional reconfigurable transmit-reflect-array using a single-layer slot element with PIN diodes," *IEEE Trans. Antennas Propag.*, vol. 67, no. 9, pp. 6205–6210, Sep. 2019.

[22] A. Massa *et al.*, "Designing smart electromagnetic environments for next-generation wireless communications," *Telecom*, vol. 2, no. 2, pp. 213–221, May 2021.

[23] J. Zhou, L. Kang, B. Tang, B. Tang, J. Huang, and C. Wang, "Adaptive compensation of flexible skin antenna with embedded fiber Bragg grating," *IEEE Trans. Antennas Propag.*, vol. 67, no. 7, pp. 4385–4396, Jul. 2019.

[24] K. Deb, A. Pratap, S. Agarwal, and T. Meyarivan, "A fast and elitist multiobjective genetic algorithm: NSGA-II," *IEEE Trans. Evol. Comput.*, vol. 6, no. 2, pp. 182–197, Apr. 2002.

[25] A. Osipov and S. Tretyakov, *Modern Electromagnetic Scattering Theory with Applications*. Chichester, U.K.: Wiley, 2017.

[26] I. V. Lindell and A. Sihvola, *Boundary Conditions in Electromagnetics*. Hoboken, NJ, USA: Wiley, 2019.

[27] G. Oliveri, A. Gelmini, A. Polo, N. Anselmi, and A. Massa, "System-by-design multiscale synthesis of task-oriented reflectarrays," *IEEE Trans. Antennas Propag.*, vol. 68, no. 4, pp. 2867–2882, Apr. 2020.

[28] P. Rocca, M. Benedetti, M. Donelli, D. Franceschini, and A. Massa, "Evolutionary optimization as applied to inverse scattering problems," *Inverse Problems*, vol. 24, no. 12, pp. 1–41, 2009.

[29] F. H. Danufane, M. D. Renzo, J. de Rosny, and S. Tretyakov, "On the path-loss of reconfigurable intelligent surfaces: An approach based on Green's theorem applied to vector fields," *IEEE Trans. Commun.*, vol. 69, no. 8, pp. 5573–5592, Aug. 2021.

[30] *ANSYS Electromagnetics Suite—HFSS*, ANSYS, Canonsburg, PA, USA, 2019.

[31] C. A. Balanis, *Antenna Theory: Analysis and Design*. Hoboken, NJ, USA: Wiley, 2005.

[32] *Technical Specification Group Radio Access Network—Study on 3D Channel Model for LTE*, document TR 36.873, Version 12.2.0, 3GPP, Jun. 2015.

Paolo Rocca (Senior Member, IEEE) received the M.S. degree *(summa cum laude)* in telecommunications engineering and the Ph.D. degree in information and communication technologies from the University of Trento, Trento, Italy, in 2005 and 2008, respectively.

He was a Visiting Ph.D. Student with Pennsylvania State University, State College, PA, USA, and the University Mediterranea of Reggio Calabria, Reggio Calabria, Italy, in 2012, and a Visiting Researcher with the Laboratoire des Signaux et Systèmes (L2S@Supèlec), France, in 2013. He has been an Invited Professor with the University of Paris Sud, Orsay, France, in 2015, and the University of Rennes 1, Rennes, France, in 2017. He is currently an Associate Professor with the Department of Civil, Environmental, and Mechanical Engineering, University of Trento, the Huashan Scholar Chair Professor with Xidian University, Xi'an, China, and a member of the ELEDIA Research Center. He is the author/coauthor of one book chapter, 150 journal articles, and more than 270 conference papers. His main interests are in the framework of artificial intelligence techniques as applied to electromagnetics, antenna array synthesis and analysis, and electromagnetic inverse scattering.

Dr. Rocca is also a member of the Big Data and AI Working Group for the Committee on Engineering for Innovative Technologies (CEIT) of the World Federation of Engineering Organizations (WFEO). He received the National Scientific Qualification for the position of a Full Professor in Italy and France in April 2017 and January 2020, respectively. He has been awarded by the IEEE Geoscience and Remote Sensing Society and the Italy Section the Best PhD Thesis Award of the IEEE-GRS Central Italy Chapter. He has served as an Associate Editor for the IEEE ANTENNAS AND WIRELESS PROPAGATION LETTERS from 2011 to 2016 and the *Microwave and Optical Technology Letters* from 2019 to 2020. He has been serving as an Associate Editor for the *IEEE Antennas and Propagation Magazine* since 2020 and *Engineering* since 2020.

Pietro Da Rù received the B.Sc. degree in telecommunications and electronics engineering and the M.Sc. degree in communication and information engineering from the University of Trento, Trento, Italy, in 2018 and 2021, respectively, where he is currently pursuing the Ph.D. degree with the Doctoral Programme in Civil, Environmental and Mechanical Engineering of Trento.

He is currently a Researcher with the ELEDIA Research Center, University of Trento. His research activity is focused on the analysis of metasurfaces and antenna arrays for next-generation communication applications.

Nicola Anselmi (Senior Member, IEEE) received the master's degree in telecommunication engineering from the University of Trento, Italy, in 2012, and the Ph.D. degree from the International Doctoral School in Information and Communication Technology, Trento, in 2018.

He is currently an Assistant Professor with the Department of Civil, Environmental, and Mechanical Engineering (DICAM), University of Trento, where he is also a Research Fellow of the ELEDIA Research Center. His research activities are mainly focused on synthesis methods for unconventional antenna array architectures, tolerance analysis of antenna systems, and electromagnetic inverse scattering techniques, with an interest in compressive sensing methodologies for microwave imaging applications.

Dr. Anselmi is also a member of the IEEE Antennas and Propagation Society. In 2019, he received the Italian National Scientific Qualification for the position of an Associate Professor and the Qualification aux Fonctions de Maître de Conférences. He was a recipient of the Giorgio Barzilai Award for Young Researchers by the Italian Electromagnetic Society (SIEM) in 2016, the Young Scientist Prize by the Applied Computational Electromagnetics Society (ACES) in 2018, and the Mini?Circuits Harvey Kaylie Best Paper Prize by the IEEE International Conference on Microwaves, Communications, Antennas & Electronic Systems (COMCAS) in 2019. He has been serving as a Reviewer for different international journals, including IEEE TRANSACTIONS ON ANTENNAS AND PROPAGATION, IEEE ANTENNAS AND WIRELESS PROPAGATION LETTERS, and *IET Microwaves, Antennas & Propagation*.

Marco Salucci (Senior Member, IEEE) received the M.S. degree in telecommunication engineering from the University of Trento, Trento, Italy, in 2011, and the Ph.D. degree from the International Doctoral School in Information and Communication Technology, Trento, in 2014.

He was a Post-Doctoral Researcher with CentraleSupélec, Paris, France, and a the Commissariat à l'Énergie Atomique et aux Énergies Alternatives (CEA), France. He is currently a Researcher with the University of Trento, where he is also a member of the ELEDIA Research Center. His research activities are mainly concerned with inverse scattering, biomedical, and GPR microwave imaging techniques, antenna synthesis, and computational electromagnetics with a focus on system-by-design methodologies integrating optimization techniques, and learning-by-examples methods for real-world applications.

Dr. Salucci was a member of the COST Action TU1208 "Civil Engineering Applications of Ground Penetrating Radar." He is also a member of the IEEE Antennas and Propagation Society. He is also an Associate Editor of Communications and Memberships of the IEEE TRANSACTIONS ON ANTENNAS AND PROPAGATION. He also serves as an Associate Editor for the IEEE TRANSACTIONS ON ANTENNAS AND PROPAGATION and a Reviewer for different international journals, including IEEE TRANSACTIONS ON ANTENNAS AND PROPAGATION, IEEE ANTENNAS AND WIRELESS PROPAGATION LETTERS, IEEE JOURNAL ON MULTISCALE AND MULTIPHYSICS COMPUTATIONAL TECHNIQUES, and *IET Microwaves, Antennas & Propagation*.

Giacomo Oliveri (Senior Member, IEEE) received the B.S. and M.S. degrees in telecommunications engineering and the Ph.D. degree in space sciences and engineering from the University of Genoa, Genoa, Italy, in 2003, 2005, and 2009, respectively.

He was a Visiting Researcher with the Laboratoire des Signaux et Systèmes (L2S)@CentraleSupélec, Gif-sur-Yvette, France, in 2012, 2013, and 2015, an Invited Associate Professor with the University of Paris Sud, Orsay, France, in 2014, and a Visiting Professor with the Université Paris-Saclay, Gif-sur-Yvette, from 2016 to 2017. He is currently an Associate Professor with the University of Trento, Trento, Italy, where he is also a Board Member of the ELEDIA Research Center. He is also an Adjunct Professor with CentraleSupélec, Paris, France, and a member of L2S. He is the author/coauthor of over 400 peer-reviewed papers in international journals and conferences. His research work is mainly focused on electromagnetic direct and inverse problems, system-by-design and metamaterials, and antenna array synthesis.

Dr. Oliveri is also the Chair of the IEEE AP/ED/MTT North Italy Chapter. He also serves as an Associate Editor for the IEEE ANTENNAS AND WIRELESS PROPAGATION LETTERS, the IEEE JOURNAL ON MULTISCALE AND MULTIPHYSICS COMPUTATIONAL TECHNIQUES, *EPJ Applied Metamaterials*, the *International Journal of Antennas and Propagation*, the *International Journal of Distributed Sensor Networks*, the *Microwave Processing* journal, and the *Sensors* journal.

Danilo Erricolo (Fellow, IEEE) received the Laurea degree *(summa cum laude)* in electronics engineering from the Politecnico di Milano, Milan, Italy, in 1993, and the Ph.D. degree in electrical engineering and computer science (EECS) from the University of Illinois Chicago (UIC), Chicago, IL, USA, in 1998.

During summer 2009, he was an Air Force Faculty Fellow with the Air Force Research Laboratory, Wright-Patterson Air Force Base, Dayton, OH, USA. He is currently a Professor and the Director of Graduate Studies of the Department of Electrical and Computer Engineering, the Director of the Andrew Electromagnetics Laboratory, and an Adjunct Professor of bioengineering with UIC. He has authored or coauthored more than 290 publications in refereed journals and international conferences. His research interests are primarily in the areas of antenna design, electromagnetic propagation and scattering, high-frequency techniques, wireless communications, electromagnetic compatibility, the computation of special functions, and magnetic resonance imaging.

Dr. Erricolo was an elected Full Member of Commissions B, C, and E of the U.S. National Committee (USNC) of the International Union of Radio Science (URSI) and the Committee of the U.S. National Academies. In 2017, he was nominated as a University of Illinois Scholar. He was an elected member of the IEEE AP-S Administrative Committee from 2012 to 2014. He was the Chair of the IEEE AP-S Distinguished Lecturer Program from 2015 to 2016 and the Chicago Joint Chapter of the IEEE AP-S and Microwave Theory and Techniques Society from 2011 to 2016. He has served as the Chair from 2009 to 2011, the Vice-Chair from 2006 to 2008, and the Secretary from 2004 to 2005 of the USNC-URSI Commission E on Electromagnetic Environment and Interference. He was the Chair of the USNC-URSI Ernest K. Smith Student Paper Competition from 2009 to 2014, the Vice-Chair of the Local Organizing Committee of the XXIX URSI General Assembly, held in Chicago, in August 2008, and a member at large of USNC-URSI from 2012 to 2017. He was the General Chairman of the 2012 IEEE International Symposium on Antennas and Propagation and the USNC-URSI National Radio Science Meeting, held in Chicago, in July 2012. He has served on more than 50 conference technical program committees, chaired over 70 conference sessions, and organized more than 30 special sessions at international scientific conferences. He has been the Editor-in-Chief of the IEEE TRANSACTIONS ON ANTENNAS AND PROPAGATION since August 2016.

Andrea Massa (Fellow, IEEE) received the Laurea (M.S.) degree in electronic engineering and the Ph.D. degree in electrical engineering and computer science (EECS) from the University of Genoa, Genoa, Italy, in 1992 and 1996, respectively.

He is currently the Director of the Network of Federated Laboratories, 'ELEDIA Research Center," Brunei, China, Czech, France, Greece, Italy, Japan, Peru, and Tunisia, with more than 150 researchers. He is also a Chang-Jiang Chair Professor with the University of Electronic Science and Technology of China (UESTC), Chengdu, China, a Professor with CentraleSupélec, Paris, France, and a Visiting Professor with Tsinghua University, Beijing, China. He has been holder of the Senior DIGITEO Chair at the Laboratoire des Signaux et Systèmes (L2S), CentraleSupélec, and LIST, Commissariat à l'Énergie Atomique et aux Énergies Alternatives (CEA), Saclay, France, the UC3M-Santander Chair of Excellence with the Universidad Carlos III de Madrid, Madrid, Spain, an Adjunct Professor with Penn State University, State College, PA, USA, a Guest Professor with UESTC, and a Visiting Professor with the Missouri University of Science and Technology, Rolla, MO, USA, Nagasaki University, Nagasaki, Japan, the University of Paris Sud, Orsay, France, Kumamoto University, Kumamoto, Japan, and the National University of Singapore, Singapore. He is also a Full Professor of electromagnetic fields with the University of Trento, Trento, Italy, where he currently teaches electromagnetic fields, inverse scattering techniques, antennas and wireless communications, wireless services and devices, and optimization techniques. He has published more than 900 scientific publications among which more than 350 in international journals (more than 13 500 citations—H-index = 60 [Scopus]; more than 11 000 citations—H-index = 54 [ISI-WoS]; and more than 22 000 citations—H-index = 87 [Google Scholar]) and more than 550 in international conferences where he presented more than 200 invited contributions (more than 40 times as an invited keynote speaker). He has organized more than 100 scientific sessions in international conferences and has participated in several technological projects in the national and international framework with both national agencies and companies (18 international projects, >5 M€; eight national projects, >5 M€; ten local projects, >2 M€; 63 industrial projects, >10 M€; and six university projects, >300 k€). His research activities are mainly concerned with inverse problems, analysis/synthesis of antenna systems and large arrays, radar systems synthesis and signal processing, cross-layer optimization and planning of wireless/RF systems, semantic wireless technologies, system-by-design and material-by-design (metamaterials and reconfigurable-materials), and theory/applications of optimization techniques to engineering problems (telecommunications, medicine, and biology).

Dr. Massa is also an IET Fellow and an Electromagnetic Academy Fellow. He is also a member of the Editorial Board of the *Journal of Electromagnetic Waves and Applications*, a Permanent Member of the PIERS Technical Committee and the EuMW Technical Committee, and an ESoA Member. He also serves as Associate Editor for the *International Journal of Microwave and Wireless Technologies*. He was appointed to the Scientific Board of the "Società Italiana di Elettromagnetismo (SIEm)" and elected to the Scientific Board of the Interuniversity National Center for Telecommunications (CNIT). He was appointed in 2011 by the National Agency for the Evaluation of the University System and National Research (ANVUR) as a member of the Recognized Expert Evaluation Group (Area 09, Industrial and Information Engineering) for the evaluation of the research at the Italian University and Research Center for the period 2004–2010. He was elected as the Italian Member of the Management Committee of the COST Action TU1208 "Civil Engineering Applications of Ground Penetrating Radar." He was appointed as the IEEE AP-S Distinguished Lecturer from 2016 to 2018. He has served as an Associate Editor for the IEEE TRANSACTIONS ON ANTENNAS AND PROPAGATION from 2011 to 2014.